AEDC-TR-77-47

AN EXPERIMENTAL AND ANALYTIC INVESTIGATION OF A TRANSONIC SHOCK-WAVE/BOUNDARY-LAYER INTERACTION

PROPULSION WIND TUNNEL FACILITY
ARNOLD ENGINEERING DEVELOPMENT CENTER
AIR FORCE SYSTEMS COMMAND
ARNOLD AIR FORCE STATION, TENNESSEE 37389

May 1977

Final Report for Period July 1, 1975 - June 30, 1976

Prepared for

DIRECTORATE OF TECHNOLOGY
ARNOLD ENGINEERING DEVELOPMENT CENTER
AIR FORCE SYSTEMS COMMAND
ARNOLD AIR FORCE STATION, TENNESSEE 37389

NOTICES

When U. S. Government drawings specifications, or other data are used for any purpose other than a definitely related Government procurement operation, the Government thereby incurs no responsibility nor any obligation whatsoever, and the fact that the Government may have formulated, furnished, or in any way supplied the said drawings, specifications, or other data, is not to be regarded by implication or otherwise, or in any manner licensing the holder or any other person or corporation, or conveying any rights or permission to manufacture, use, or sell any patented invention that may in any way be related thereto.

Qualified users may obtain copies of this report from the Defense Documentation Center.

References to named commercial products in this report are not to be considered in any sense as an endorsement of the product by the United States Air Force or the Government.

This report has been reviewed by the Information Office (OI) and is releasable to the National Technical Information Service (NTIS). At NTIS, it will be available to the general public, including foreign nations.

APPROVAL STATEMENT

This technical report has been reviewed and is approved for publication.

FOR THE COMMANDER

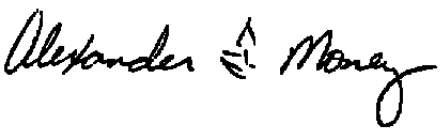

ALEXANDER F. MONEY
Research and Development
Division
Directorate of Technology

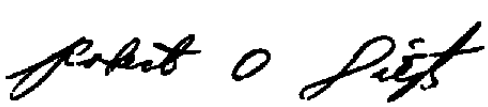

ROBERT O. DIETZ
Director of Technology

REPORT DOCUMENTATION PAGE		READ INSTRUCTIONS BEFORE COMPLETING FORM
1 REPORT NUMBER AEDC-TR-77-47	2 GOVT ACCESSION NO.	3. RECIPIENT'S CATALOG NUMBER
4. TITLE (and Subtitle) AN EXPERIMENTAL AND ANALYTIC INVESTIGATION OF A TRANSONIC SHOCK-WAVE/BOUNDARY-LAYER INTERACTION		5 TYPE OF REPORT & PERIOD COVERED Final Report - July 1, 1975 - June 30, 1976 6 PERFORMING ORG. REPORT NUMBER
7 AUTHOR(s) M. C. Altstatt, ARO, Inc.		8 CONTRACT OR GRANT NUMBER(s)
9 PERFORMING ORGANIZATION NAME AND ADDRESS Arnold Engineering Development Center (DY) Air Force Systems Command Arnold Air Force Station, Tennessee 37389		10. PROGRAM ELEMENT PROJECT, TASK AREA & WORK UNIT NUMBERS Program Element 65807F
11 CONTROLLING OFFICE NAME AND ADDRESS Arnold Engineering Development Center (DYFS) Air Force Systems Command Arnold Air Force Station, Tennessee 37389		12 REPORT DATE May 1977 13 NUMBER OF PAGES 40
14 MONITORING AGENCY NAME & ADDRESS(if different from Controlling Office)		15. SECURITY CLASS. (of this report) UNCLASSIFIED 15a DECLASSIFICATION/DOWNGRADING SCHEDULE N/A

16 DISTRIBUTION STATEMENT (of this Report)

Approved for public release; distribution unlimited.

17. DISTRIBUTION STATEMENT (of the abstract entered in Block 20, if different from Report)

18 SUPPLEMENTARY NOTES

Available in DDC

19 KEY WORDS (Continue on reverse side if necessary and identify by block number)

boundary layer	computations	high speed photography
shock waves	pressure	transonic flow
separation	profiles	wind tunnel tests
interactions	laser velocimeters	

20 ABSTRACT (Continue on reverse side if necessary and identify by block number)

Two wind tunnel tests were conducted in a flow exhibiting a shock-wave/boundary-layer interaction of the type occurring on airfoils at transonic velocities. Boundary-layer pressure distributions were measured with pitot and static probes. Velocities in the free stream and in the boundary layer were obtained with a laser velocimeter (LV) system, and a data reduction program for the LV results was developed. Measurements from the pressure probes and from the LV system are compared with each other and

DD FORM 1 JAN 73 1473 EDITION OF 1 NOV 65 IS OBSOLETE

20. ABSTRACT (Continued)

with theoretical computations. It was found that the analytic models for boundary-layer velocity profile and Reynolds stress agree well with experimental measurements.

PREFACE

The research reported herein was performed by the Arnold Engineering Development Center (AEDC), Air Force Systems Command (AFSC), under Program Element 65807F. Work and analysis for this research was done by personnel of ARO, Inc., AEDC Division (a Sverdrup Corporation Company), operating contractor of AEDC, AFSC, Arnold Air Force Station, Tennessee. The work was conducted under ARO Project No. P32A-C1A. The author of this report was M. C. Altstatt, ARO, Inc. The manuscript (ARO Control No. ARO-PWT-TR-77-22) was submitted for publication on March 28, 1977.

CONTENTS

ILLUSTRATIONS

APPENDIX

1.0 INTRODUCTION

In transonic wind tunnel testing of airfoils, the Reynolds number scaling presents a difficult problem because of the complex interaction of the shock wave with the boundary layer. Generally, flow separation is induced at or near the shock and this separation, in turn, affects the location of the shock wave. In order to predict the aerodynamic coefficients of a wing, especially the moment coefficient, an accurate prediction of the shock location is necessary. The difficulty in predicting the change in this location with change in Reynolds number reflects an inadequate understanding of the physical phenomena and therefore in the equations used to describe these phenomena.

To provide the basic data required to evaluate certain computational methods, two wind tunnel tests were conducted. The data obtained included pitot pressure profiles in the boundary layer and laser velocimeter (LV) measurements in the boundary layer and free stream. A computer program has been developed to reduce the LV data, with emphasis on detecting and minimizing sources of measurement biasing.

Computational results for a turbulent compressible boundary layer, obtained using several different Reynolds stress models, are compared with the experimental results. The calculations are not accurate where pressure gradients are large or near flow separation. However, the models used for Reynolds stress and boundary-layer velocity produce results which do compare well with experimental data, if based on measured boundary-layer thickness and skin friction.

2.0 EXPERIMENTAL PROGRAM

Two tests were conducted in the Aerodynamic Wind Tunnel (1T). A sketch of the test section arrangement is shown in Fig. 1. The model is a circular arc bump, modified by a cosine fairing at each end, mounted on the tunnel bottom wall. Testing was conducted at a nominal Mach number of 0.8 and a unit Reynolds number of approximately five million per foot. The pressure distribution and velocity, as measured by surface static ports, are shown in Fig. 2a. From Fig. 2a and the shadowgraph, Fig. 2b, it can be seen that this is a transonic flow of the type desired, with a shock-wave/boundary-layer interaction and flow separation. The supercritical region extends from approximately station 18 to 21, where the shock occurs. The separation point is at about station 21.75.

2.1 TESTING

For the first test, 22 pitot pressure profiles were obtained in the boundary layer. The probes were projected through the tunnel bottom wall and positioned by an electric drive. High-speed shadowgraph motion pictures were taken to determine the flow stability. At 400 frames per second the boundary layer, shock position, and separation point appeared to be stationary on the surface, but at a height of above 2 in. the shock was oscillating slightly.

In the second test, a laser velocimeter system, described in Ref. 1, was used to measure flow velocity profiles at 19 boundary-layer profiles and four streamwise paths through the shock. The program developed for the LV data reduction is described in the Appendix. A streamwise coordinate system is used for all the LV boundary-layer results presented.

2.2 TEST RESULTS

For direct comparison of pitot and LV velocity measurements, several boundary-layer profiles taken with the pitot probe in the first test were repeated with the LV system in the second test. Figure 3a shows a typical comparison for data taken near the leading edge of the bump. There is good agreement for all profiles taken at corresponding locations in the attached flow.

In the separated region, as illustrated in Fig. 3b, the LV and pitot probe results do not agree. The LV data are preferred in the separated region because the pitot probe is affected by variations in flow angle and possible variations in local static pressure and free-stream stagnation pressure. Sources which can affect the interpretation of LV measurements, such as particle lag, velocity biasing, and time variation, are discussed in Refs. 2 and 3 and in the Appendix.

A problem in consistently interpreting the LV data arises in determining the location of the edge of the boundary layer. The pitot data give consistent criteria for the edge, as long as the free-stream stagnation pressure remains constant. With velocity data only, however, as can be seen from Fig. 3c, the boundary-layer edge is less clearly defined. This ambiguity can affect the computation of the boundary-layer properties.

Starting above the bump centerline, LV velocity surveys were conducted downstream parallel to the tunnel bottom wall. Figure 4 shows velocity and stream angle for four profiles at 1.25, 1.5, 1.75, and 2.0 in. above the bottom wall. These profiles indicate a variation from an almost normal shock at y = 2.0 in. to a family of oblique shocks at the surface.

The LV data presented in this report were processed by a data reduction program which is described in the Appendix. Information,

such as mode, standard deviation, skewness, kurtosis, and covariance, is extracted from the LV velocity measurements. As defined in Ref. 4, the standard deviation and covariance are directly related to the turbulent intensity and Reynolds stress. The mode, skewness, and kurtosis are assessed for evidence of biasing in the measurements.

Mean and mode velocity, turbulent intensity, and Reynolds stress profiles in the separated flow at station 23.88 are shown in Fig. 5. Because of the flow fluctuation in this region and the length of time required to obtain these measurements, the accuracy may be poor near the surface.

3.0 THEORETICAL ANALYSIS

Computations were performed for the boundary layer measured, using the experimental pressure distribution as an input. The solution was compared with the test data to determine the accuracy of the theoretical solutions and evaluate available turbulence models.

3.1 BOUNDARY-LAYER CALCULATION METHOD

The calculation method used for a turbulent, compressible boundary layer is a variation of the method of Nash and Hicks (Ref. 5) as modified by Kuhn and Nielsen (Ref. 6). The formulation and computer code used are reported in Ref. 7.

A summary of the equations is given below.

Continuity

$$\frac{\partial}{\partial x}(\rho u) + \frac{\partial}{\partial y}(\rho v) = 0 \tag{1}$$

Momentum Energy

$$\rho u \frac{\partial u}{\partial x} + \rho v \frac{\partial u}{\partial y} = - \frac{\partial p}{\partial x} + \frac{\partial}{\partial y}\left(\mu\beta \frac{\partial u}{\partial y}\right) \tag{2}$$

Energy

$$\rho u \frac{\partial S}{\partial x} + \rho v \frac{\partial S}{\partial y} = \frac{\partial}{\partial y}\left(\mu\beta \frac{\partial S}{\partial y}\right) \tag{3}$$

It is assumed that the Prandtl number is unity for both laminar and turbulent flow. In these equations, β is defined by

$$\beta = 1 + \epsilon/\nu \tag{4}$$

where ε is the eddy viscosity,

$$\epsilon = - \overline{\rho u' v'} \frac{\partial u}{\partial y} \tag{5}$$

u′ and v′ are the turbulent velocity fluctuations, and the bar denotes a time average. The enthalpy parameter, S, is given by

$$S = T/T_t - 1 \tag{6}$$

with T_t as the total temperature.

Application of the Stewartson transformations to these equations results in the set:

$$\frac{\partial U}{\partial X} + \frac{\partial V}{\partial Y} = 0 \tag{7}$$

Momentum

$$U \frac{\partial U}{\partial X} + V \frac{\partial U}{\partial Y} - \frac{\rho_e}{\rho} U_e \frac{\partial U_e}{\partial X} - \nu \frac{\partial}{\partial Y}\left(\beta \frac{\partial U}{\partial Y}\right) = 0 \tag{8}$$

The terms U, V, X, and Y are transformed, incompressible velocities, and coordinates, and the subscript e refers to conditions at the edge of the boundary layer. An adiabatic wall is assumed and Crocco's relation with a recovery factor of 0.89 is used as an empirical solution to the energy equation.

$$\frac{\rho_e}{\rho} = 1.0 + 0.178\, M_e^2 \left(1.0 - \frac{U^2}{U_e^2}\right) \tag{9}$$

Substituting Eq. (7) into Eq. (8) and integrating across the boundary layer results in

$$\int_0^{\delta} [UU_x\, U_Y \int_0^Y U_x d\eta - \frac{\rho_e}{\rho} U_e\, Ue_x - \nu\, (\beta U_Y)_Y]\; Y^n dY = 0 \tag{10}$$

where n = 0, 1.

A wall-wake model is used for the boundary-layer velocity profile,

$$U = u_\tau [2.5\, \ell n\, (1 + y^+) + 5.1 - (3.39y^+ + 5.1)_e\, ^{-0.37y^+}] + \frac{u_\beta}{2}\left(1 - \cos\frac{\pi y}{\delta}\right) \tag{11}$$

where U_τ is a friction velocity,

$$u_\tau = (1\, \tau_w\, 1/\rho)^{1/2}\; \tau_w / \tau_w \tag{12}$$

u_β is a wake velocity,

$$u_\beta = U_e - u_\tau [2.5\, \ell n\, (1 + \delta^+) + 5.1] \tag{13}$$

and

$$y^+ = u_\tau\, Y/\nu \tag{14}$$

This set of equations can be closed with a model for eddy viscosity. The inner and outer eddy viscosity models given by Alber (Ref. 8) are used:

Inner wall model

$$\beta_i = 1.0 + 0.0533\, \{e^{U^+} - [1.0 + U^+ + \tfrac{1}{2} U^{+2}]\} \tag{15}$$

where

$$U^+ = 0.41\ U/u_\tau \tag{16}$$

Outer wake model

$$\beta_o = 1.0 + 0.0168\ [1.0 + 5.5\ (Y/\delta)^6]^{-1}\ \frac{U_e S^*}{\nu} \tag{17}$$

A set of differential equations was therefore formed, in terms of u_τ and δ, and the Runge-Kutta method of advancing in the streamwise direction was used.

3.2 COMPARISON WITH EXPERIMENT

Figure 6 illustrates measured and calculated displacement thickness on the model. The agreement, as shown in Fig. 6a, is good to about tunnel station 16, where the pressure gradient is becoming large. Past that point, the computed displacement thickness deviates rapidly from the experimental values. Figure 6b shows a comparison of analytic and measured displacement thickness downstream in the region of the shock and separation. Since the solution shown in Fig. 6a became unstable past station 16, this solution was restarted at station 18. As expected, the boundary-layer solution is not accurate in this region of strong pressure gradient and flow reversal.

3.3 REYNOLDS STRESS MODELS

In order to determine the sensitivity of the solutions to the modeling of the Reynolds stress term in Eq. (10), several expressions for the eddy viscosity were used. These forms are

Moses (Ref. 9)

$$\beta = \frac{U_e \theta}{\nu}\ (0.0225 + 125.0/R_\delta) \tag{18}$$

Michael-Quemard-Durant (Ref. 9)

$$\epsilon = F^2 \ell^2 \frac{\partial U}{\partial Y} \tag{19}$$

$$F = 1.0 - e^{-\frac{u_\tau Y}{0.0855}} \tag{20}$$

$$\ell = 0.085\,\delta \tanh\left(\frac{0.41Y}{0.085\,\delta}\right) \tag{21}$$

Lees (modified) (Ref. 8)

$$\epsilon_o = 0.018\, U_e Y \left(1.0 - \frac{U^2}{U_e^2}\right) \tag{22}$$

$$\epsilon_i = \epsilon_o (Y/Y_\nu)^2 \tag{23}$$

A laminar case ($\epsilon = 0$) was also run. In the cases for which no inner model is given, Eq. (15) is used.

A comparison of the resulting Reynolds stresses (β) is given in Fig. 7. Although these models show substantial differences in β distribution, the effect is small on the computation of displacement thickness, for the region near the bump LE, as shown in Fig. 8. Also, downstream of station 16 the solution becomes unstable regardless of the eddy viscosity model. The local variations across the boundary layer are smoothed by the integration process.

3.4 VERIFICATION OF ANALYTIC MODELS

Results from the models used for the boundary-layer velocity profiles [Eq. (11)] and Reynolds stress [Eqs. (15) and (17)] can be compared directly with experimental measurements. Figures 9a and b illustrate such a comparison at tunnel station 14.5. Even though the agreement between the calculated and experimental values shown is very good, it is

at about this point where the downstream advance by the boundary-layer scheme begins to deviate sharply from the measured boundary layer. This deviation may exist because the momentum balance for the streamwise advance is inappropriate in the large pressure gradient.

As noted above, the boundary-layer scheme is not valid in the shock-separation region downstream. However, at locations where experimental data are available, Eqs. (11) through (17) can be used with the measured, integrated boundary-layer properties as input, and velocity profiles and Reynolds stress computed, as in starting solutions. Figures 9c and d show a comparison of these computations with the measured velocity and Reynolds stress. It can be seen that even though the calculation is not valid in the downstream direction, the models used in the equations are consistent with experimental data at a given station. Therefore, the boundary-layer equations utilized are suspect in this region.

4.0 CONCLUSIONS

An investigation of a transonic flow containing a shock-wave/boundary-layer interaction of the type occurring on airfoils was conducted, using both experimental and theoretical methods. Tests were conducted in the Aerodynamic Wind Tunnel (1T). Data included surface static pressures, high-speed shadowgraph motion pictures, and pitot pressure profiles in the boundary layer. A laser velocimeter system was used to obtain velocity measurements in the boundary layer and in the free stream. A data reduction program was developed to extract mode and mean velocity, standard deviation, skewness, kurtosis, and Reynolds stress from the velocity measurements.

A program for a turbulent, compressible boundary layer was used to compute the boundary-layer properties for the flow field investigated. A comparison of the analytic and experimental displacement thickness shows good agreement in attached flows except in regions with large pressure gradients and near the separation point.

An investigation was initiated to determine the accuracy of some of the turbulence models used. Several eddy viscosities were used in the computation of Reynolds stress for the boundary-layer equations. Even though the various Reynolds stresses calculated were substantially different, the resulting differences in displacement thickness were relatively small. The integral boundary-layer scheme smooths out the local variations in eddy viscosity.

A comparison of the computed and measured Reynolds stresses and boundary-layer velocity profiles at selected points shows good agreement, even where the computed boundary-layer results are deviating from the measured values. The set of boundary-layer equations used is apparently inadequate for the regions of strong pressure gradient.

In the separated region to the rear of the shock, good agreement can also be obtained between the computed and measured Reynolds stresses and velocities if experimental data are used as input in the calculation. Even though the method of solution for the boundary layer is inaccurate, the turbulence models are self-consistent at any given station.

REFERENCES

1. Cline, V. A. and Lo, C. F. "Application of the Dual-Scatter Laser Velocimeter in Transonic Flow Research." AGARD Meeting on Applications of Nonintrusive Instrumentation in Fluid Flow Research, France, May 1976.

2. Lo, C. F. and Heltsley, F. L. "Interpretation of Laser Velocimeter Measurements in a Transonic Flow Field." 22nd ISA Aerospace Instrumentation Symposium, San Diego, California, May 1976.

3. Karpuk, M. E. and Tiederman, W. G., Jr. "Effect of Finite-Size Probe Volume upon Laser Doppler Anemometer Measurements." AIAA Journal, Vol. 14, No. 8, August 1976, pp. 1099-1105.

4. Tennekes, H. and Lumley, J. L. A First Course in Turbulence. M.I.T. Press, Cambridge, Massachusetts, 1972.

5. Nash, J. F. and Hicks, J. G. "An Integral Method Including the Effect of Upstream History on the Turbulent Shear Stress." Proceedings, 1968 AFOSR-IPF-Stanford Conference on Computation of Turbulent Boundary Layers, Stanford University, 1968, Vol. 1, 1969, pp. 37-45.

6. Kuhn, G. D. and Nielsen, J. N. "Prediction of Turbulent Separated Boundary Layers." AIAA Journal, Vol. 12, No. 7, July 1974.

7. Altstatt, M. C. "Evaluation of a Method for Computation of Separated Turbulent, Compressible Boundary Layers." AEDC-TR-76-27 (AD-A021090), February 1976.

8. Alber, I. E. "Similarity Solutions for a Family of Separated Turbulent Boundary Layers." AIAA Paper No. 71-203, 9th Aerospace Sciences Meeting, New York, N. Y., January 1971.

9. Moses, Hal L. "A Strip-Integral Method for Predicting the Behavior of Turbulent Boundary Layers." Proceedings, AFSOR-IFP-Stanford Conference on Computation of Turbulent Boundary Layers, Stanford University, 1968, Vol. 1, 1969, pp. 76-82.

10. Lo, C. F., Heltsley, F. L., and Altstatt, M. C. "A Study of Laser Velocimeter Measurements in a Transonic Flow." AIAA Paper No. 76-333, AIAA 9th Fluid and Plasma Dynamics Conference, San Diego, California, July 1976.

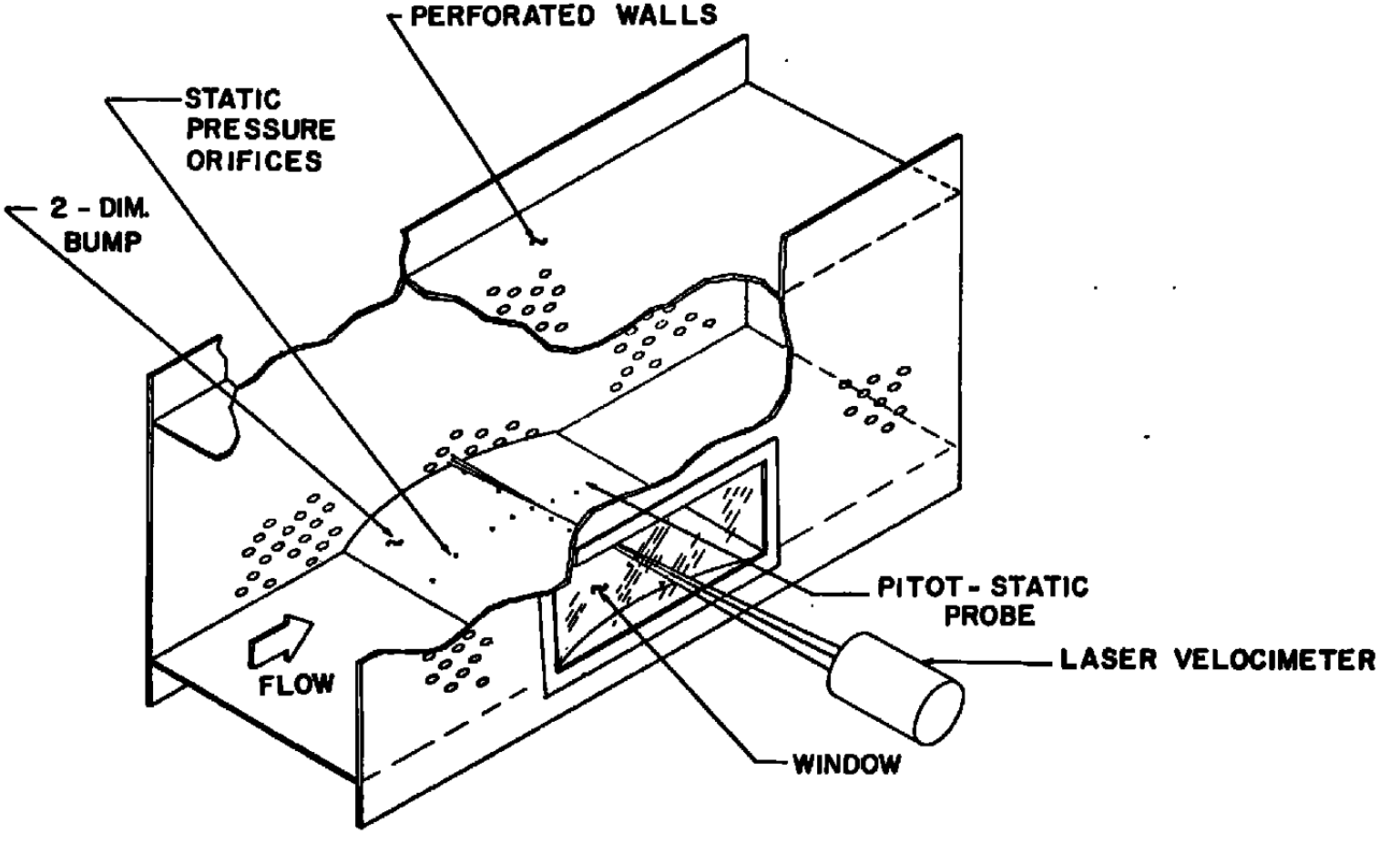

Figure 1. Test section arrangement.

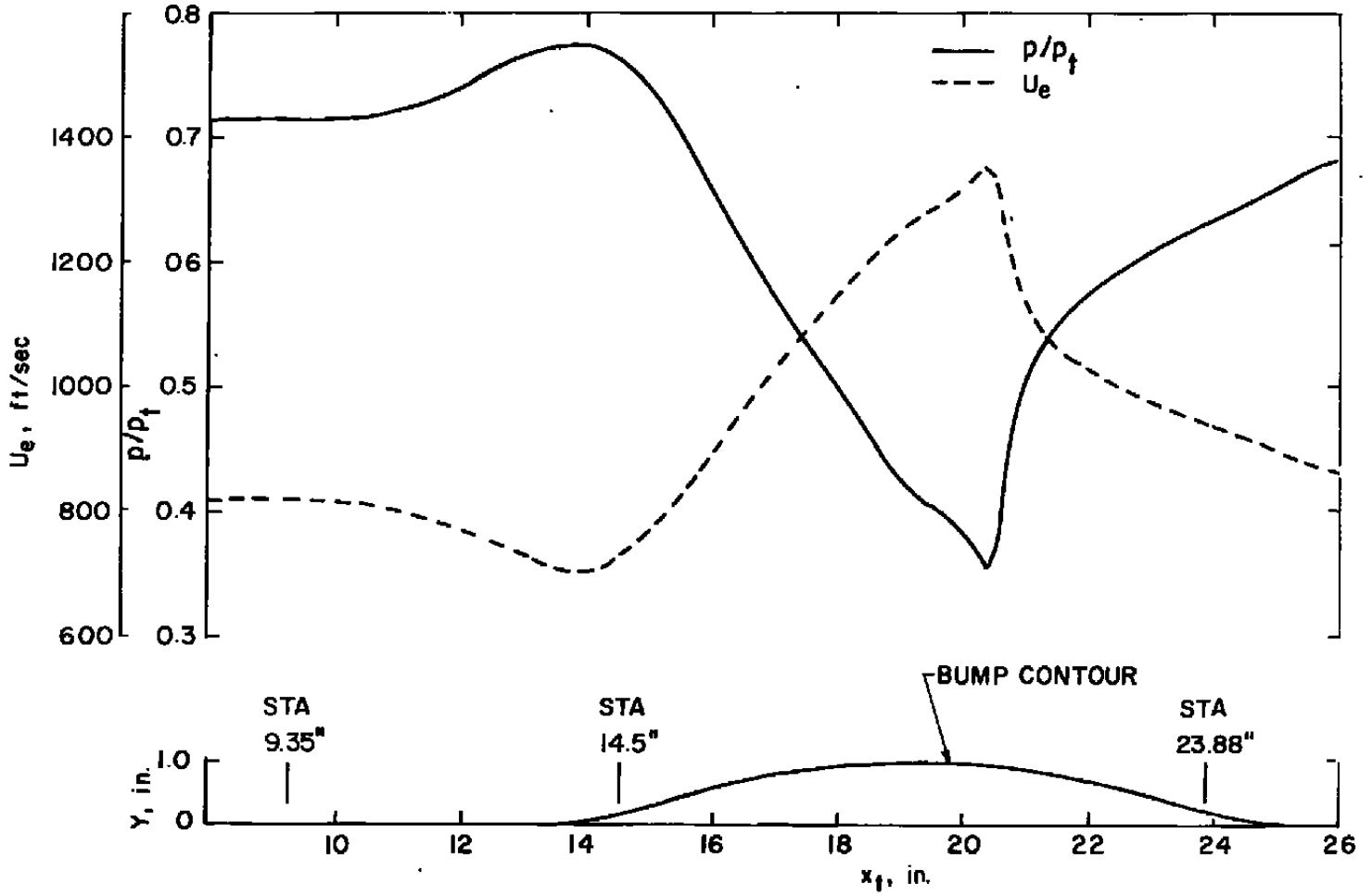

a. Pressure distribution and velocity

Figure 2. Flow field.

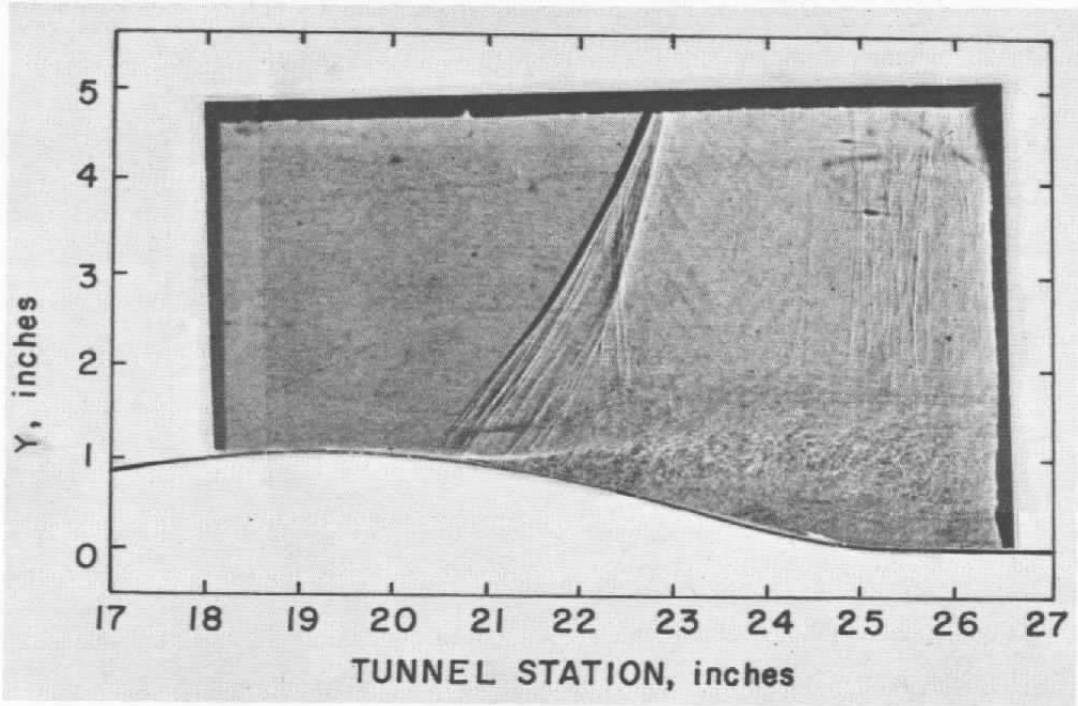

b. Shadowgraph
Figure 2. Concluded.

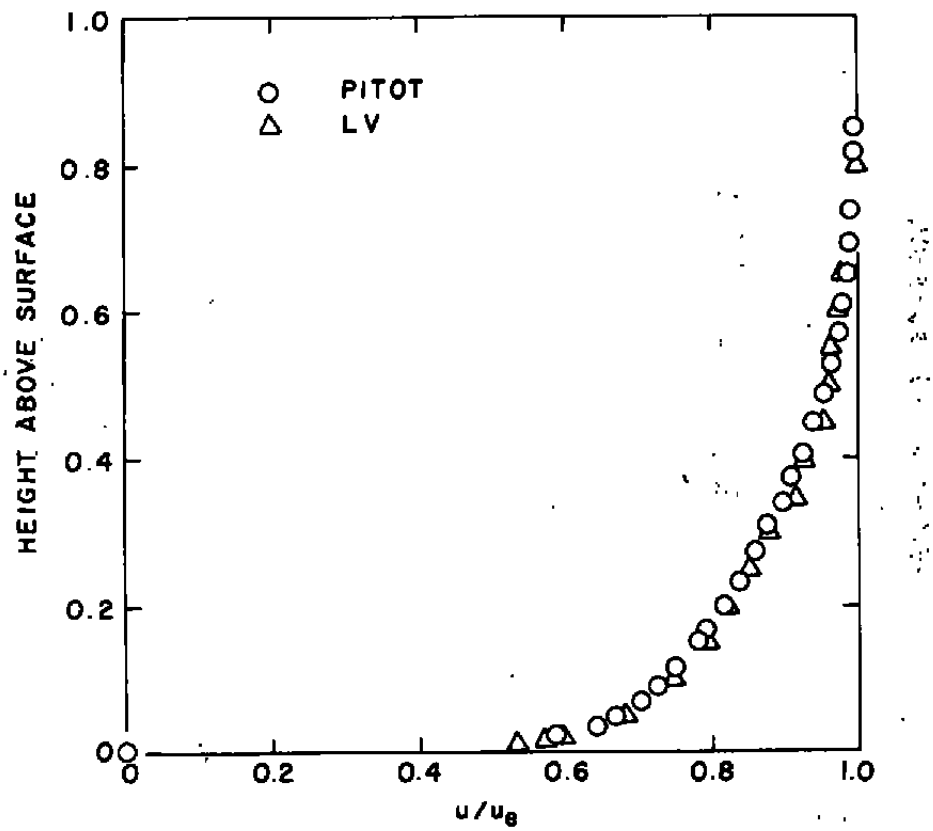

a. Velocities upstream of the model, station 9.35

Figure 3. Comparison of laser velocimeter and pitot tube measurements in the boundary layer.

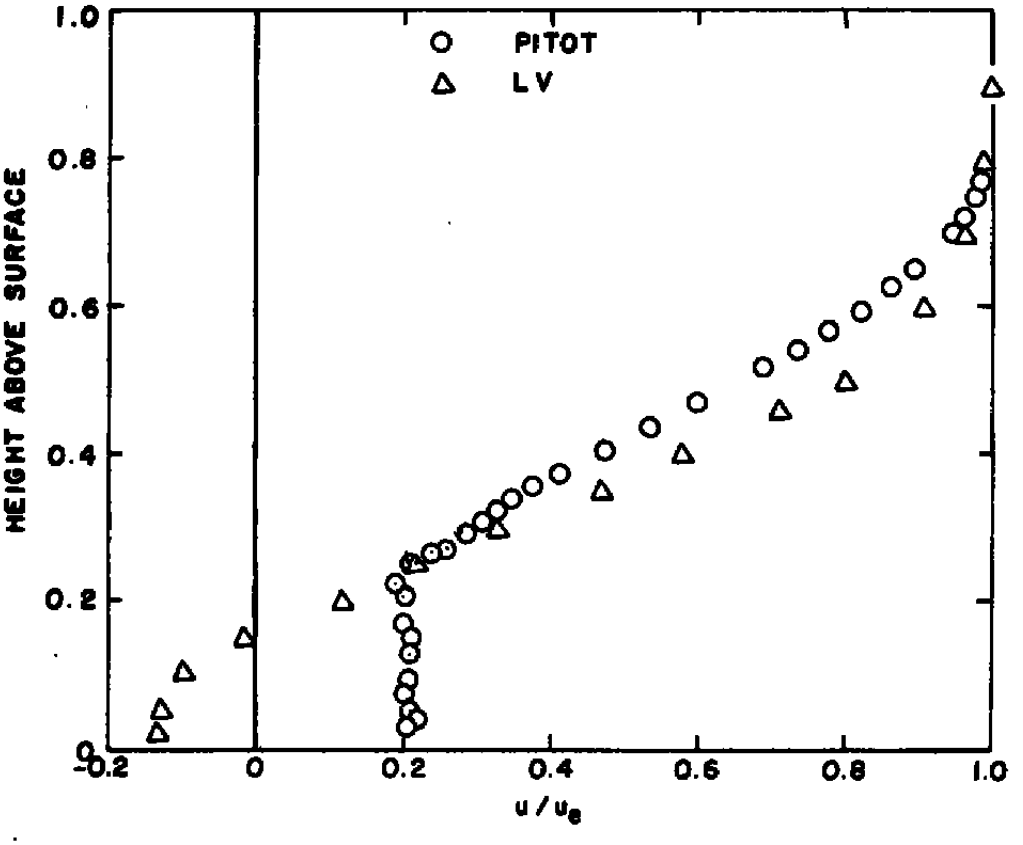

b. Velocities in separated flow, station 23.88
Figure 3. Continued.

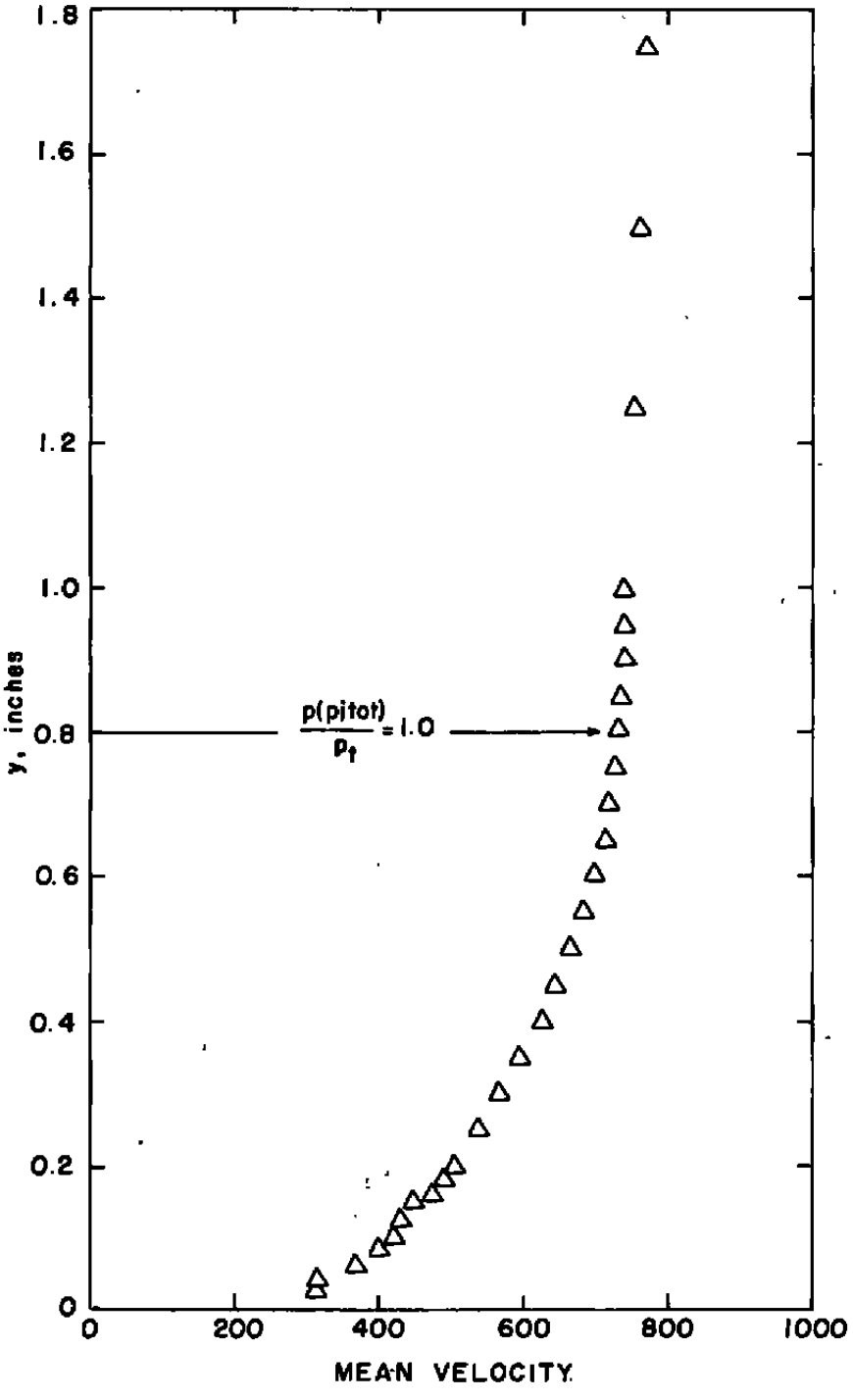

c. Boundary-layer thickness, station 13.5
Figure 3. Concluded.

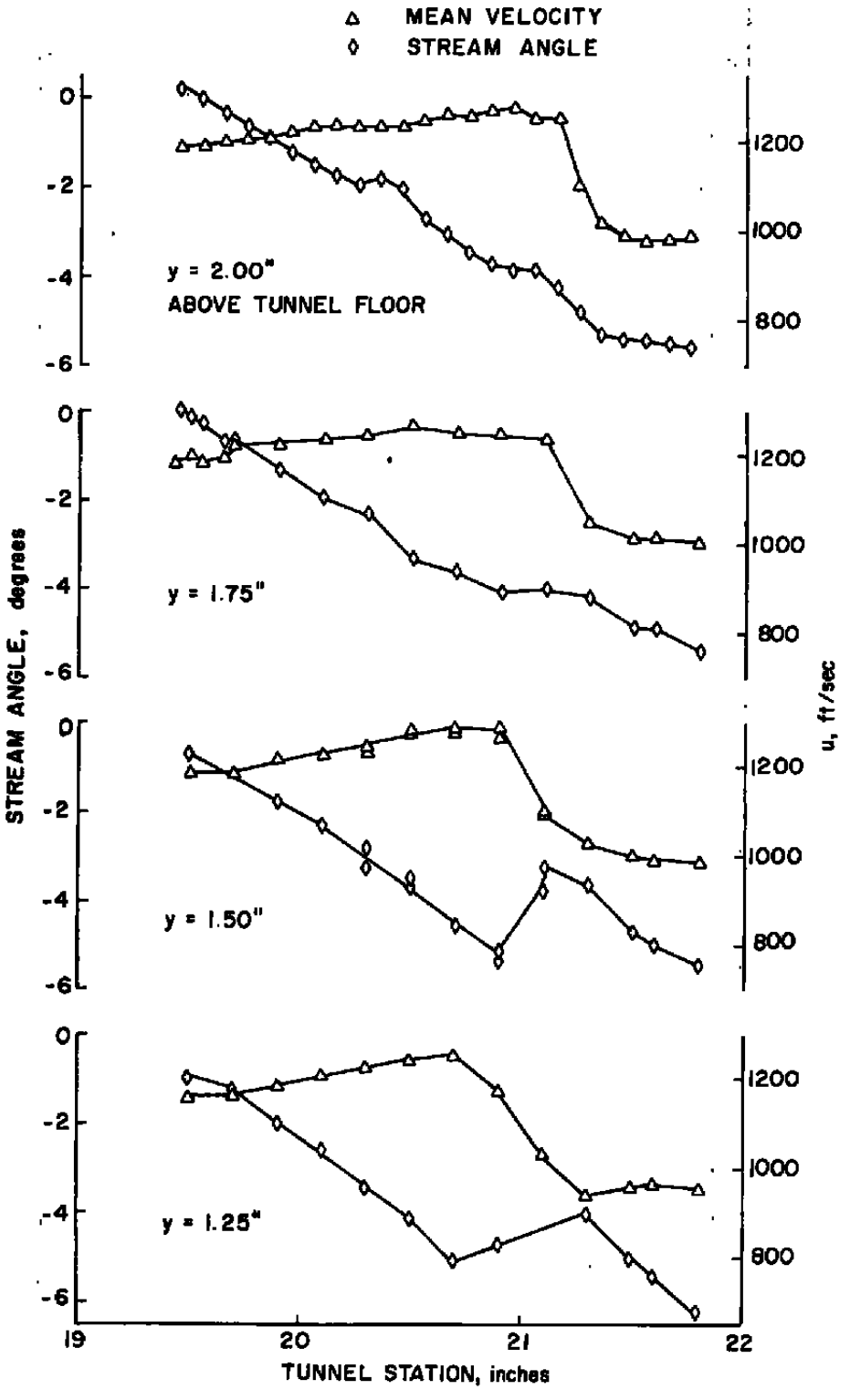

Figure 4. Velocity profiles through the shock wave.

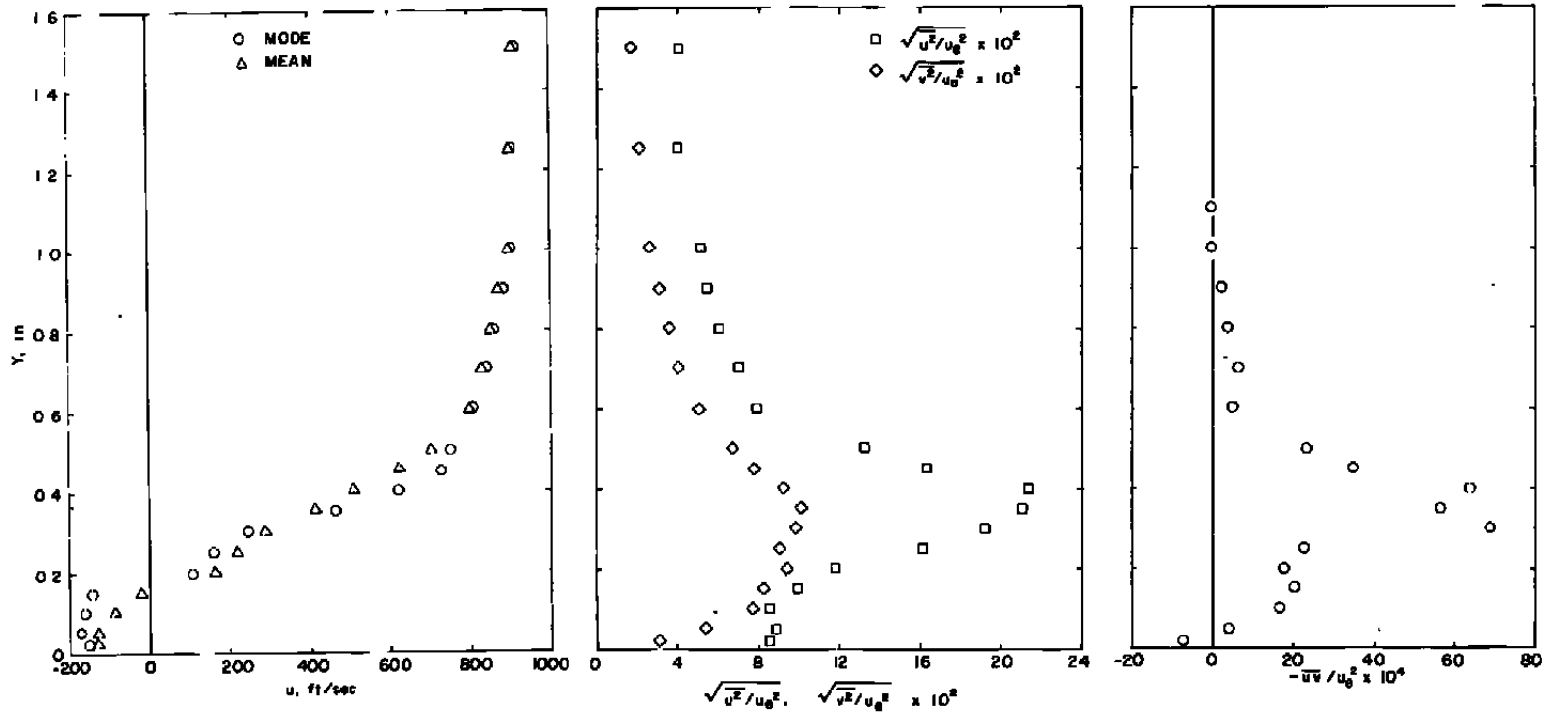

a. Velocity profile

b. Turbulent intensity

c. Reynolds stress

Figure 5. Boundary-layer properties.

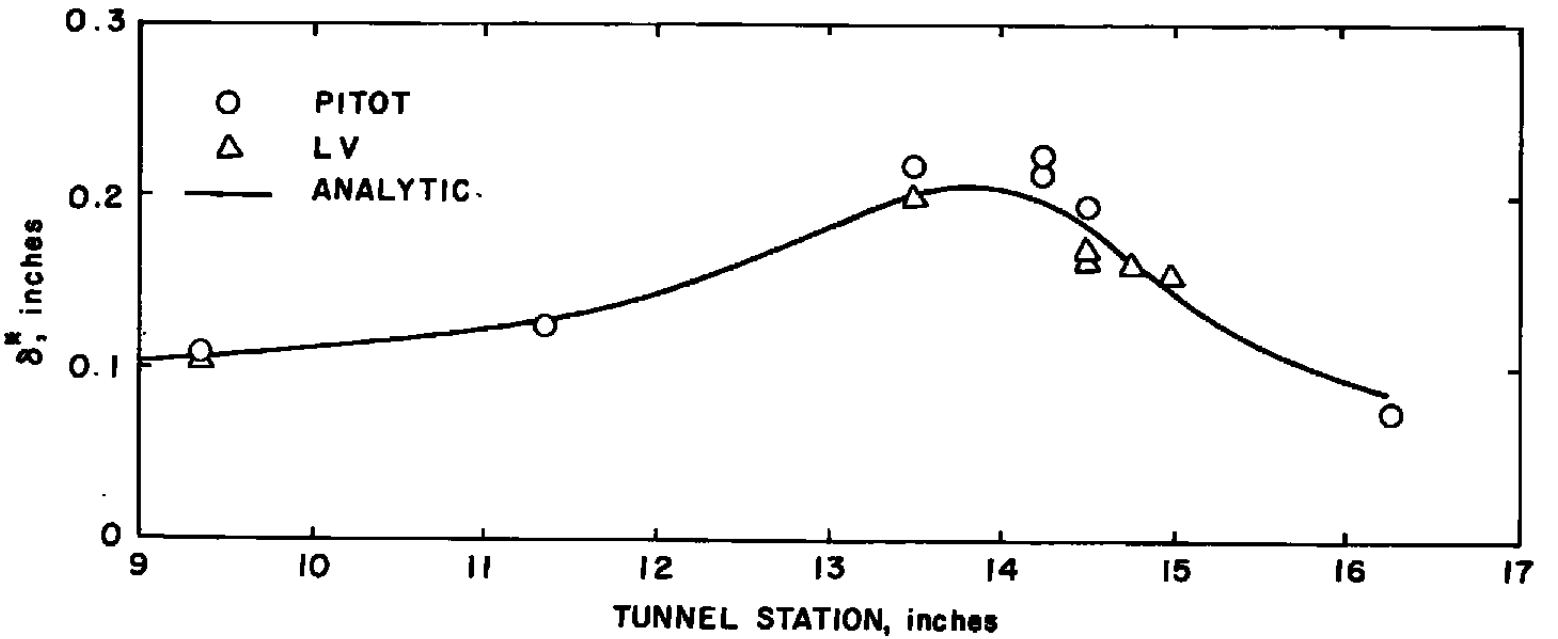

a. Attached boundary-layer region

Figure 6. Experimental and computed displacement thickness.

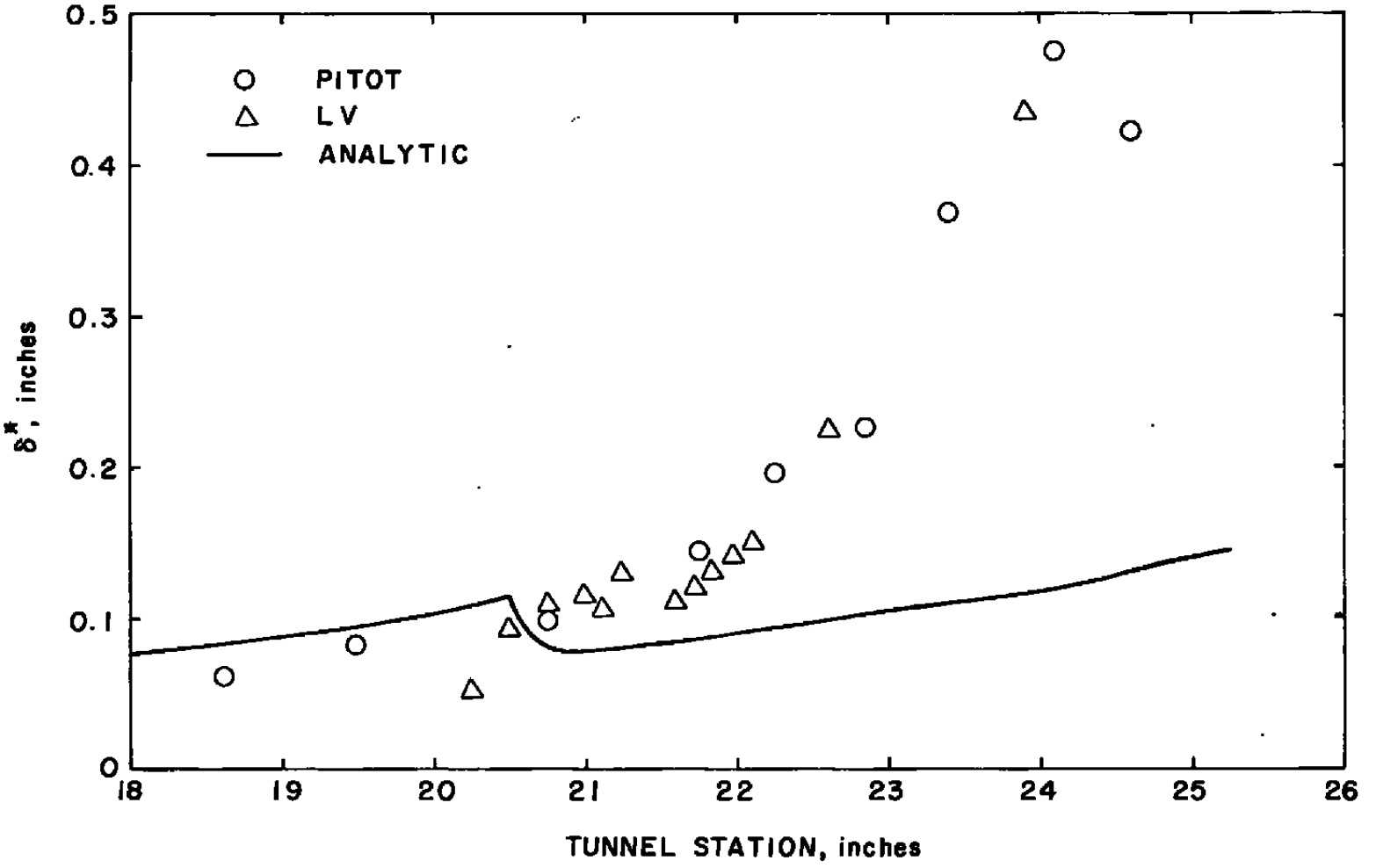

b. Shock wave/boundary-layer interaction and separation regions

Figure 6. Concluded.

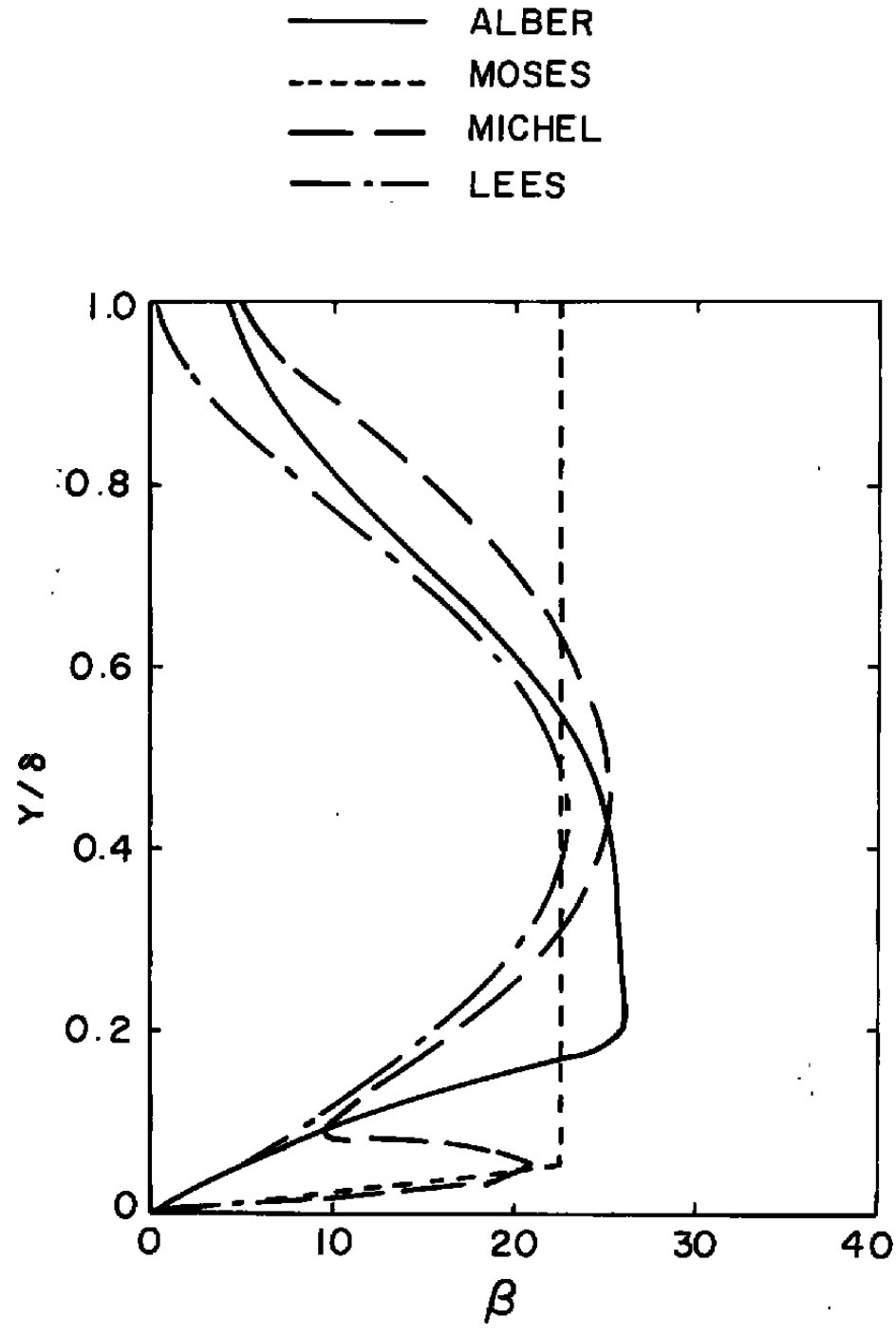

Figure 7. Comparison of Reynolds stress models (β), station 14.5.

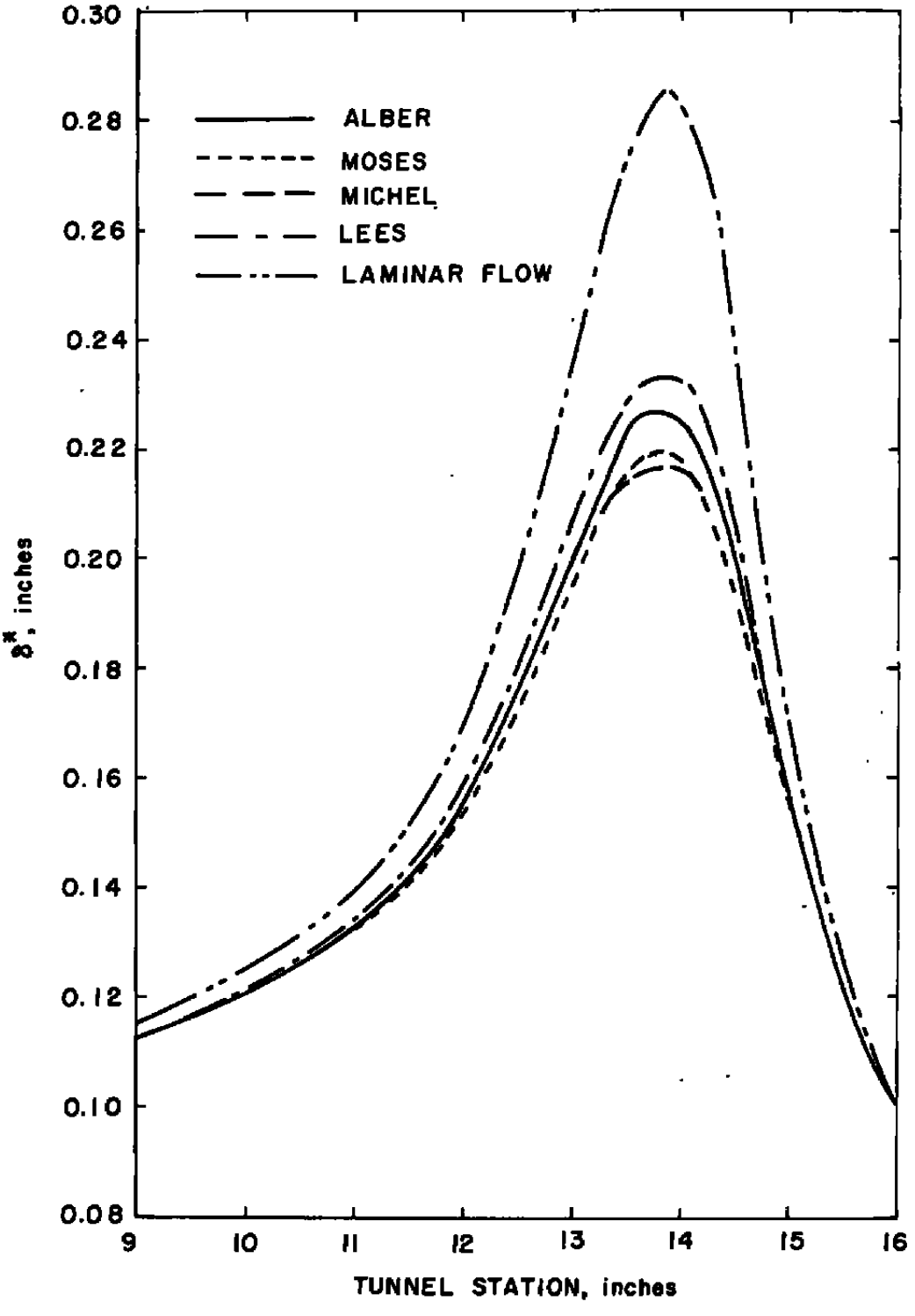

Figure 8. Computed displacement thicknesses with several Reynolds stress models.

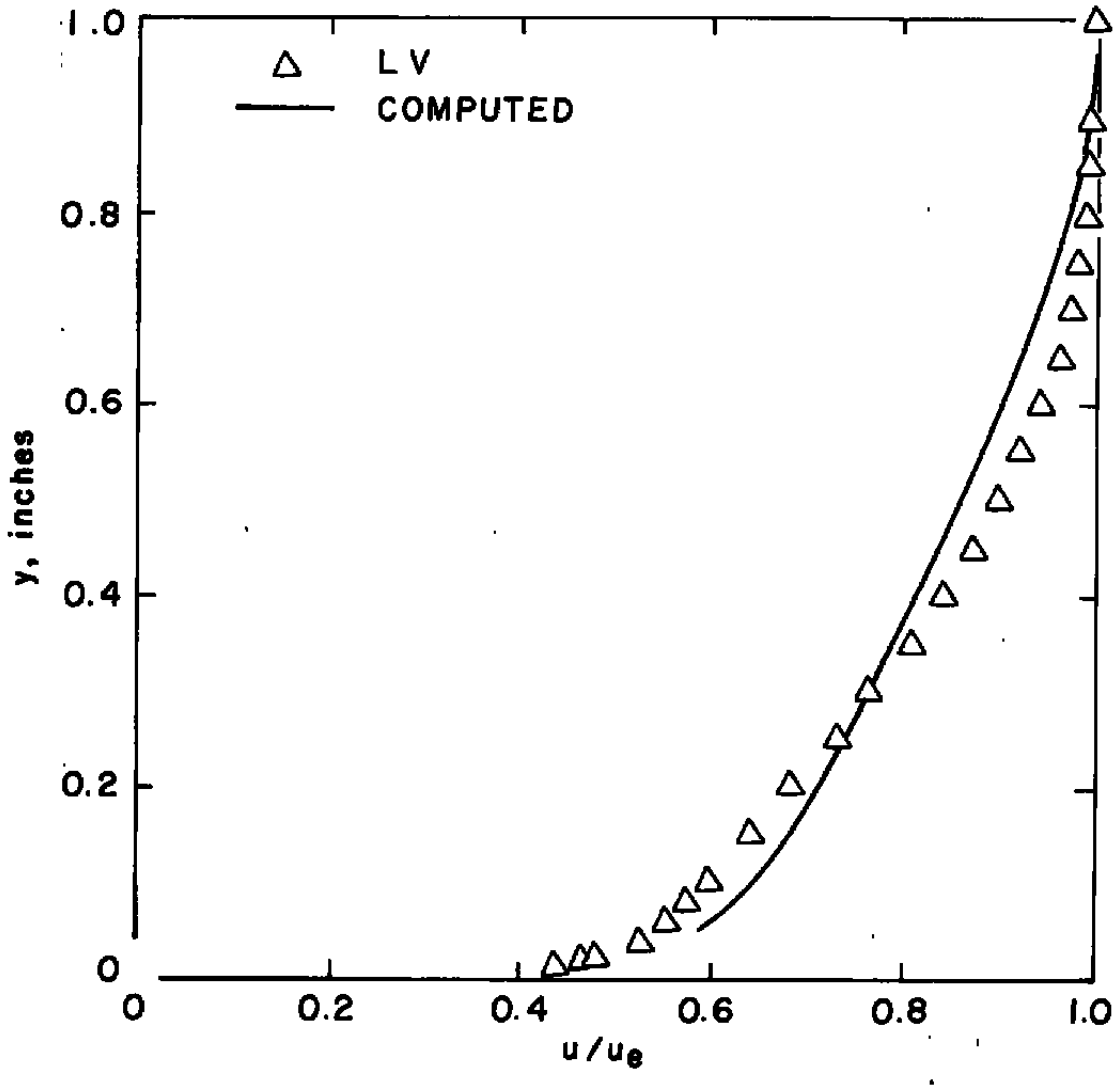

a. Velocity profile at station 14.5

Figure 9. Comparison of analytic results with experimental measurements.

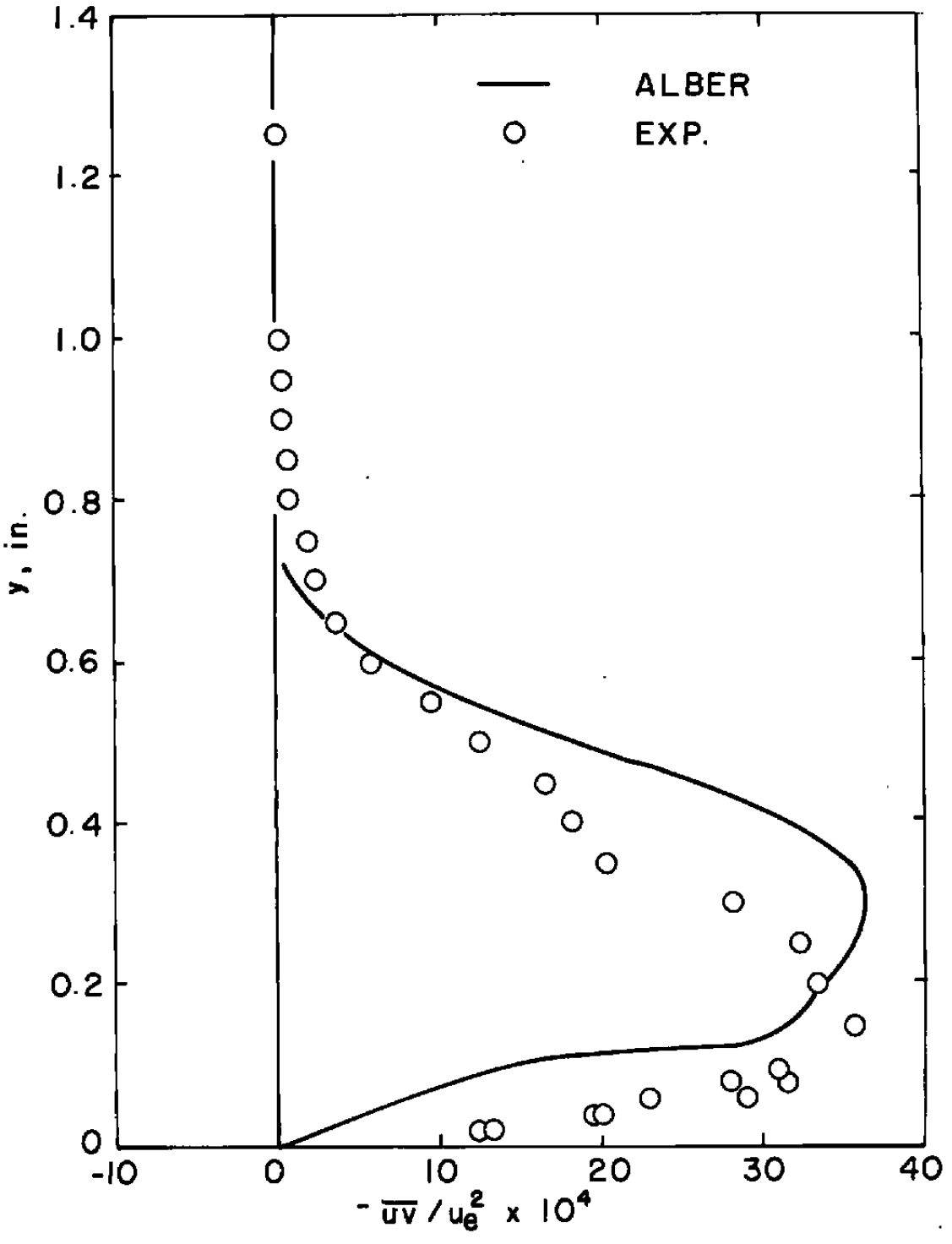

b. Reynolds stress at station 14.5

Figure 9. Continued.

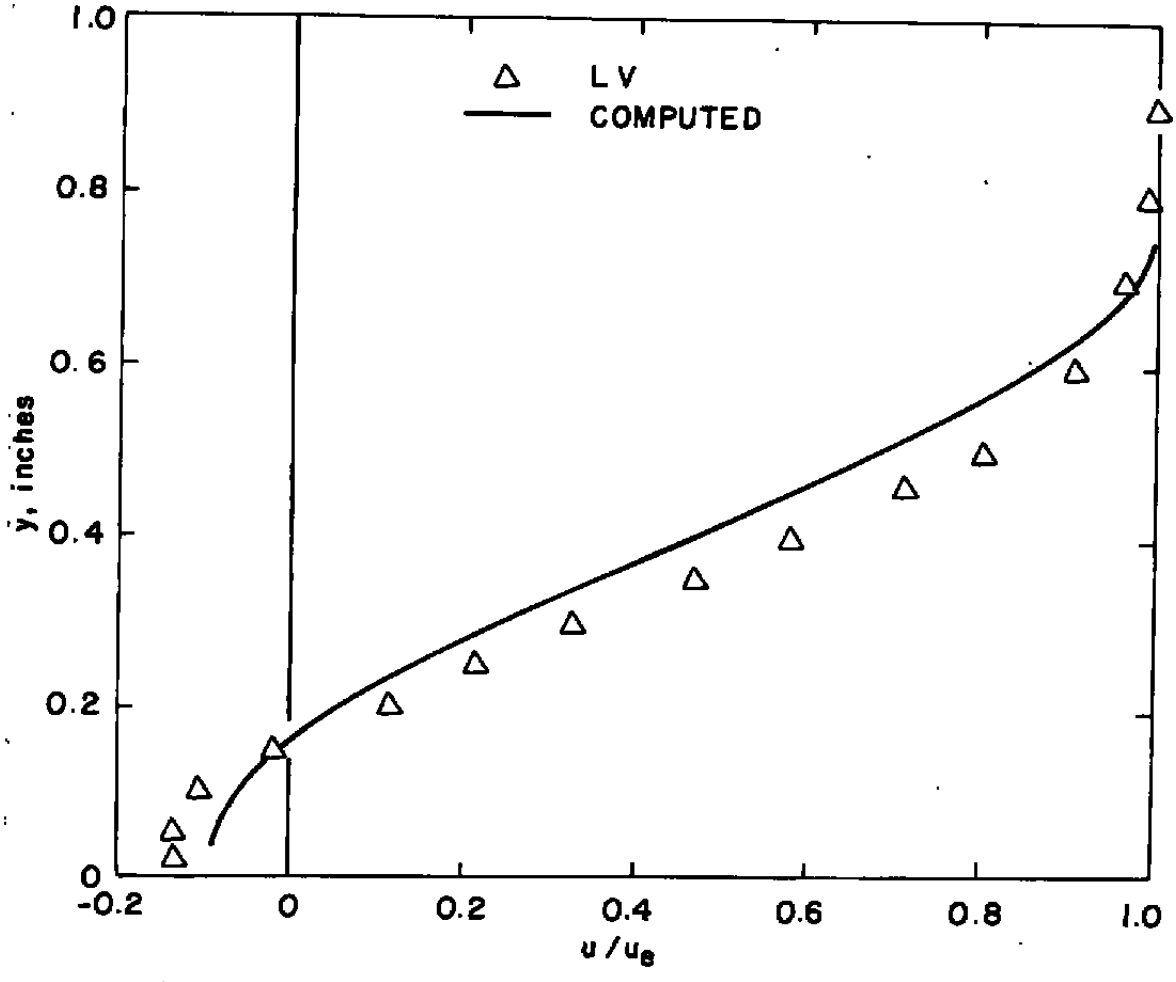

c. Velocity profile at station 23.88
Figure 9. Continued.

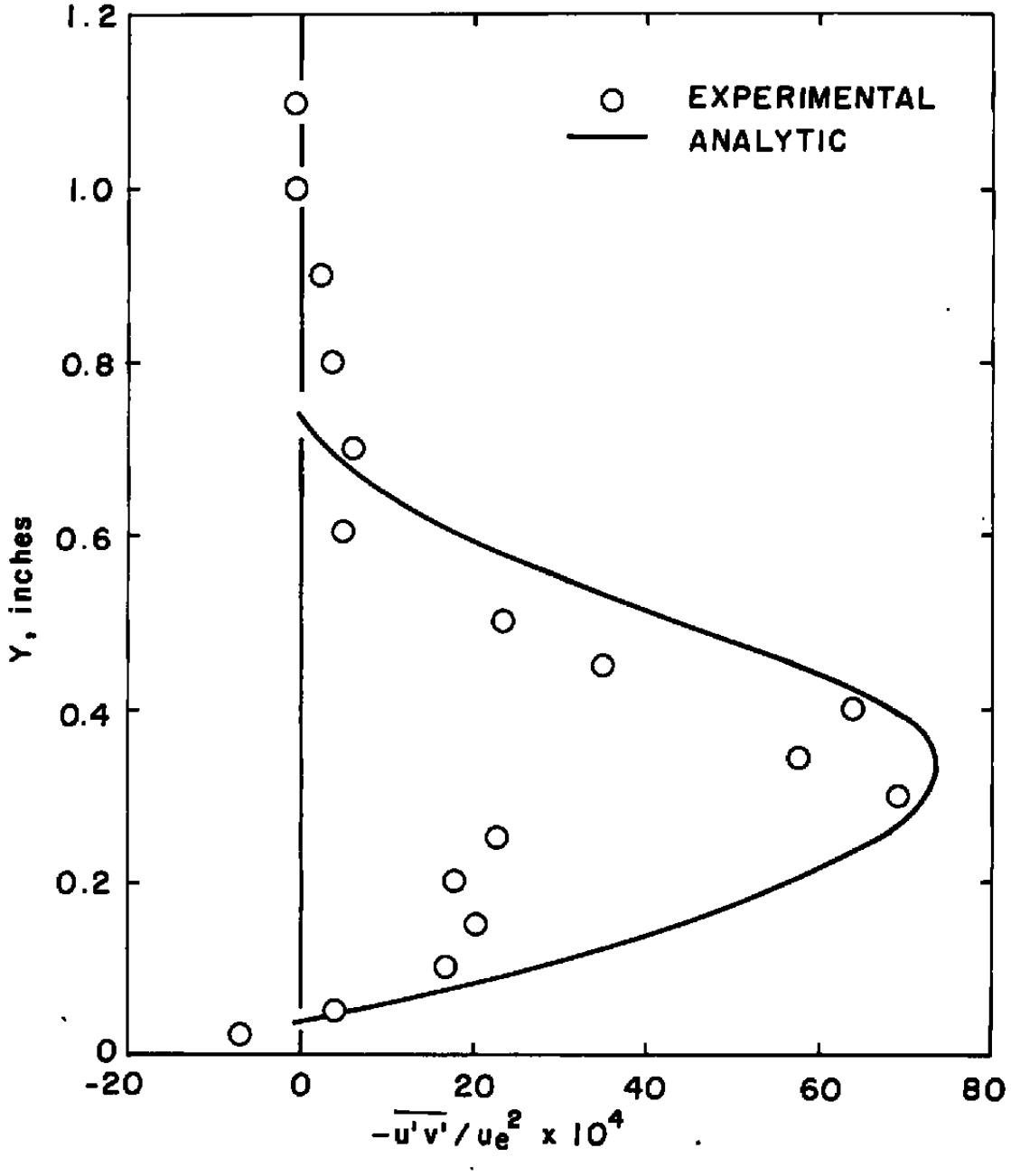

d. Reynolds stress at station 23.88
Figure 9. Concluded.

APPENDIX A
LASER VELOCIMETER DATA REDUCTION

The laser velocimeter (LV) system records two components of velocity for a particle passing through the beam intersection volume, which is approximately 0.3 mm in diameter by 9 mm in length. More details of the LV and data acquisition system are reported in Ref. 10. At a point in the flow, approximately 1,000 velocity pairs are taken. The time required to obtain the data can vary from less than a second to several minutes, depending on the number of particles per unit time passing through the flow volume. Figure A-1 illustrates a data set which is low in the boundary layer near the separation point.

DATA REDUCTION EQUATIONS

The flow characteristics computed from the LV data are mean and mode velocity, turbulent intensity, skewness, kurtosis, and Reynolds stress. The following expressions were used:

Mean velocity

$$u = \frac{1}{N} \sum_{i=1}^{N} u_i \tag{A-1}$$

Standard deviation

$$\sigma = \sqrt{\frac{1}{N} \sum_{i=1}^{N} (u_i - u)^2} \tag{A-2}$$

Skewness

$$\frac{1}{N\sigma^3} \sum_{i=1}^{N} (u_i - u)^3 \tag{A-3}$$

Kurtosis

$$\frac{1}{N\sigma^4} \sum_{i=1}^{N} (u_i - u)^4 \tag{A-4}$$

Convarience

$$\overline{u'v'} = \frac{1}{N} \sum_{i=1}^{N} (u_i - u)(v_i - v) \qquad \text{(A-5)}$$

where u_i and v_i are individual velocity samples and N is the number of samples.

To determine the mode velocity, a histogram is formed, as in Fig. A-2. Here the number of velocity samples falling within a given velocity range, usually 10 ft/sec, is plotted against velocity. A least-squares polynominal curve fit (the curve shown on the plot) is obtained, and the maximum of the curve is taken as the mode value.

DATA INTERPRETATION

Although the data reduction equations are simple, interpretation of the results presents problems. Some of the factors producing uncertainty in the results are listed below.

Tracking: In the unseeded flow used, the particle size and composition distribution is not known, so there can be an unknown difference between particle velocity and fluid velocity for the measurements.

Velocity Bias: For some combinations of velocity and particle number density, as shown in Ref. 3, the probability of obtaining high-velocity data is greater, since more high-velocity particles pass through the probe volume.

Flow Fluctuation: Because of the time required to obtain 1,000 velocity sets, if the flow is fluctuating or tunnel conditions are varying, improper readings are obtained.

Position Drift: Especially for low boundary-layer points, where position is critical and record times can be long, temperature change and vibration can produce error.

Processor Bias: The LV signal processor is biased toward certain digits in the last decimal place, which introduces an error if the standard deviation is small.

The uncertainty introduced by these factors can vary from less than 2 percent in a free-stream flow to the order of 20 percent for a boundary-layer point in a fluctuating flow. Some of the options built into the data reduction program are designed to indicate or minimize these errors.

PROCESSING OPTIONS

The data processing options in the program fall into three categories: selection of valid data, method of processing, and presentation of results.

Given a set of 1,000 two-component velocity readings, some of these will have one or both measurements misread. These bad readings are removed from the data set. Then, the data set can be further reduced by the deletion of velocity records which differ from the mean by more than some value, usually three standard deviations. Also, the data set can be reduced to simultaneous components or all velocities of each component can be processed.

The output can be presented in tunnel or streamwise coordinates or rotated to any desired angle from either system. Print options vary from a one-line summary at each point to a full print with raw data and histograms.

Variations in processing, checking for extreme values of the velocity

moments, comparing mean and mode velocities, and other indicators from the summary outputs determine which data points require additional study. In some cases, errors can be identified and corrected, or the data point is discarded.

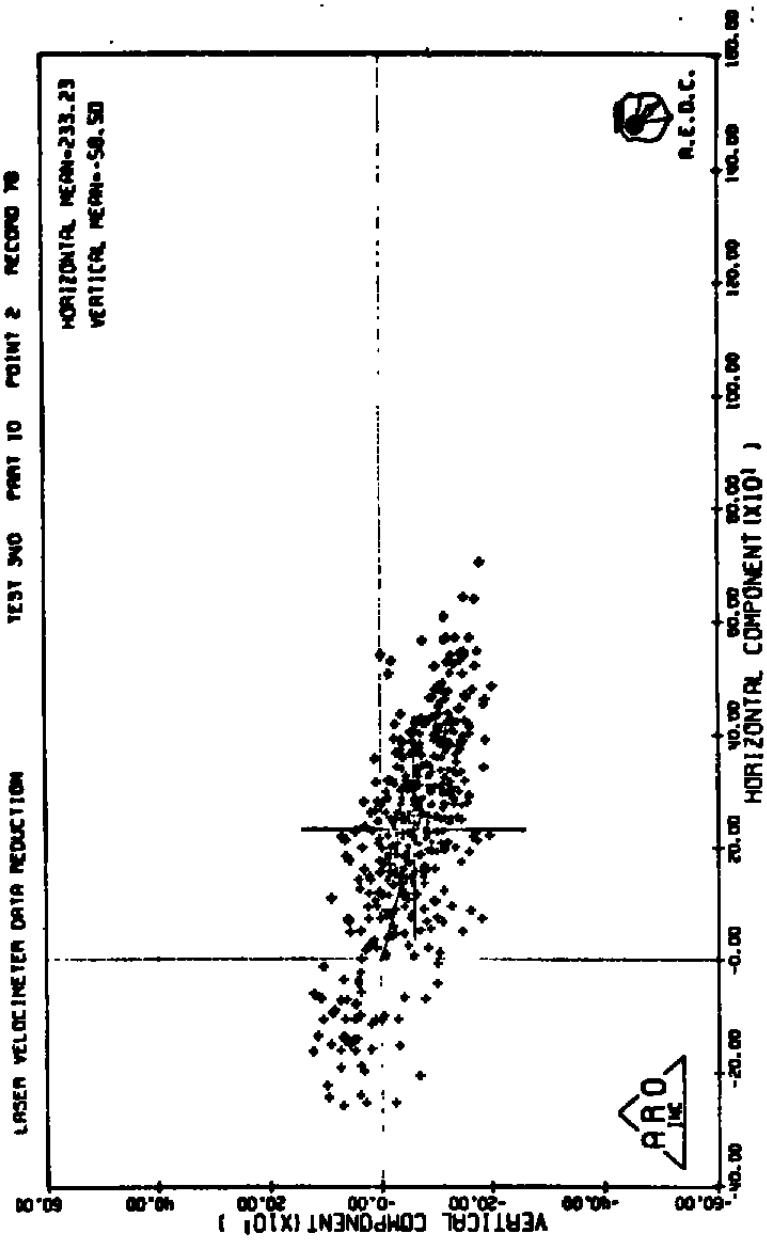

Figure A-1. Data set near the separation point.

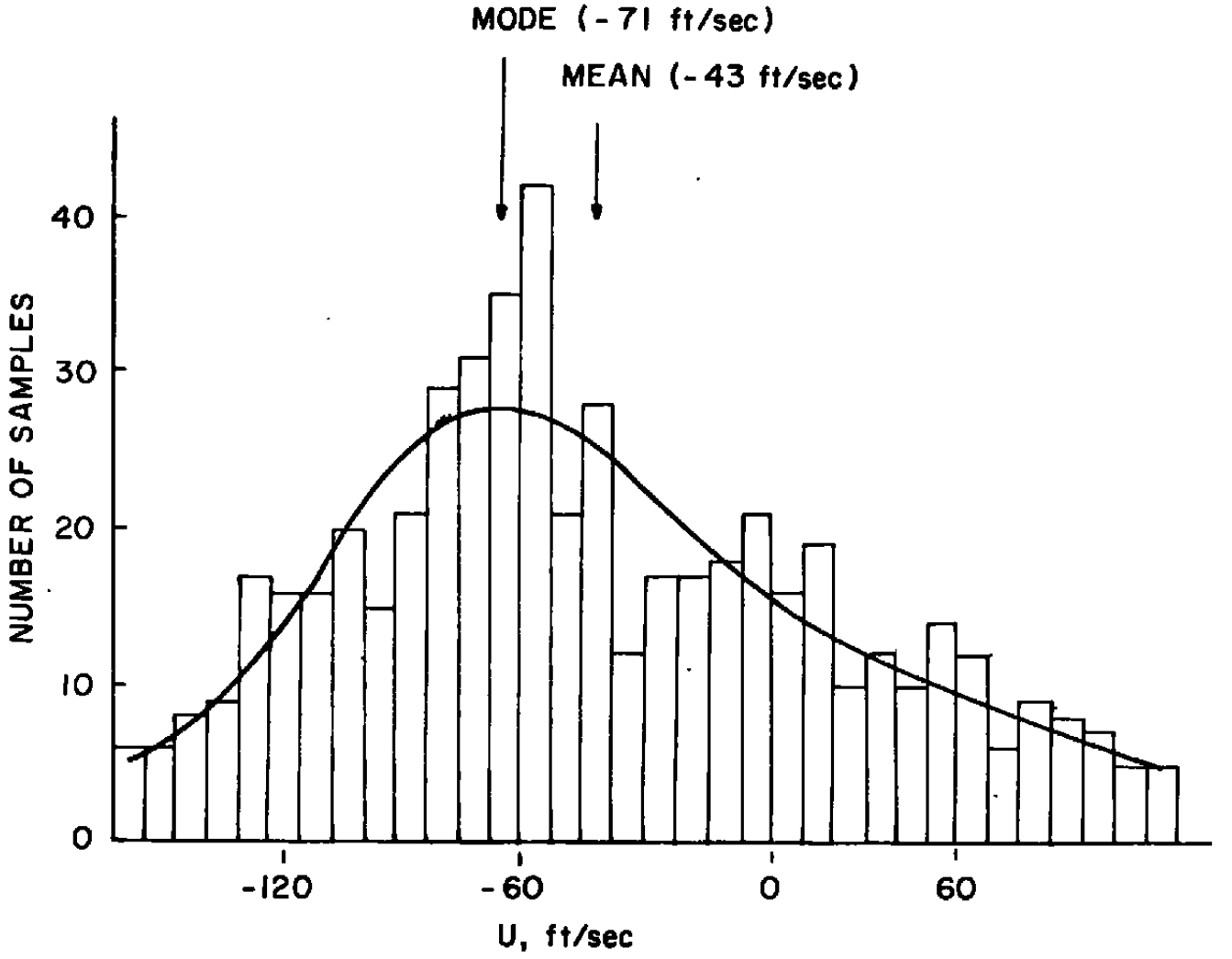

Figure A-2. Histogram showing mode velocity.

NOMENCLATURE

ℓ	Mixing length
N	Number of samples
p	Pressure
R	Reynolds number
S	Enthalpy parameter
T	Temperature
U,V	Transformed, incompressible velocities
u,v	Mean velocities
u_i, v_i	Instantaneous velocities
u', v'	Turbulent velocity fluctuations
u^+	$0.041\ U/u_t$
u_β	Wake velocity parameter
u_τ	Friction velocity parameter
X,Y	Transformed, incompressible coordinates
x,y	Physical coordinates; Y is measured from surface for boundary-layer flow, above tunnel floor otherwise; x is streamwise for boundary layers.

Y_ν	Coordinate at edge of sublayer
y^+	$u_\tau y/\nu$
β	$1 + \epsilon/\nu$
δ	Boundary-layer thickness
δ^*	Displacement thickness
ϵ	Eddy viscosity
θ	Momentum thickness
ν	Kinematic viscosity
μ	Viscosity
ρ	Density
σ	Standard deviation

SUBSCRIPTS

AW	Adiabatic wall
e	Boundary-layer edge
i	Inner
o	Outer
t	Stagnation
x,y	Partial derivative
δ	Referred to boundary-layer thickness